Modelling ultrafast laser structuring/texturing of freeform surfaces

Michalek, Aleksandra; Batal, Afif; Qi, Shaojun; Penchev, Pavel; Bruneel, David; See, Tian Long; Dimov, Stefan

Modelling ultrafast laser structuring/texturing of freeform surfaces

Aleksandra Michalek[1*], Afif Batal[1], Shaojun Qi[2], Pavel Penchev[1], David Bruneel[3], Tian Long See[4], Stefan Dimov[1]

[1]School of Mechanical Engineering, University of Birmingham, Edgbaston, Birmingham, B15 2TT, UK
[2]School of Metallurgy and Materials, University of Birmingham, Edgbaston, Birmingham, B15 2TT, UK
[3]LASEA, Rue des Chasseurs Ardennais, 10, 4031 Angleur, Belgium
[4]The Manufacturing Technology Centre Ltd, Pilot Way, Ansty Park, Coventry, CV7 9JU, UK

*Corresponding author: e-mail: AMM752@bham.ac.uk, tel.: +44 7543572512.

Abstract

Laser structuring/texturing of freeform surfaces is attracting the attention of researchers and industry because it can enable high impact applications and also the technology can offer important advantages compared to alternative/conventional processes. So far, laser structuring/texturing has been applied mostly on planar surfaces, while employing it for 3D processing it introduces some disturbances that affect the processing conditions. In particular, Beam Incident Angle (BIA) and Focal Offset Distance (FOD) variations are two important processing disturbances that impact the resulting structures/textures on freeform surfaces and also their functional responses. Furthermore, those disturbances should be considered as constraints in planning the laser processing operations, i.e. when pre-processing 3D models by partitioning into laser processing fields, and also in designing the processing strategies. However, such constraints are always material specific for a given parameters' domain and can be time-consuming to determine empirically. In this research, a model for calculating the accumulated fluence for generating Laser Induced Periodic Surface Structures (LIPSS) throughout the processed freeform surfaces is proposed. It considers the actual spatial intensity distribution of a Gaussian beam when processing 3D surfaces in the presence of varying FOD and BIA. It was demonstrated that the 3D surface processing leads to variations in their processing conditions, in particular changes of beam spot size that affect local fluence thresholds. The comparison of simulation and experimental results has shown that LIPSS main characteristics, i.e. their amplitudes and periodicity, can be predicted with acceptable accuracy. Also, changes in processing conditions caused by disturbances that affect LIPSS performance can be identified. The results of this research can be used to determine the BIA and FOD limits/tolerances within which the LIPSS functional response on freeform surfaces can be maintained within acceptable levels for any given application.

Keywords: LIPSS, freeform surface, laser processing, femtosecond laser, astigmatic Gaussian beam

1. Introduction

Laser structuring/texturing is known as advanced manufacturing process that can enhance surface properties without compromising excessively the throughput or costs. It draws the attention of researchers and industry because it offers selectivity, relatively high accuracy and flexibility, e.g. for 3D processing, when compared to alternative/conventional processes.

Laser Induced Periodic Surface Structures (LIPSS) are a particular type of submicron surface structures produced by ultrashort lasers that stand out among others due to their vast applicability and the fact that they can be generated on almost any engineering material. Firstly, they were found on semiconductors [1] but with the constant advances of ultrashort laser sources they had become a viable alternative for surface processing of metals [2]–[4], ceramics [5], metallic glasses [6], glasses [7] and polymers [8]. Because of LIPSS specific geometrical characteristics, all these materials benefit from added surface functionalities, such as improved wetting properties for self-cleaning or anti-icing applications [9], [10], anti-bacterial surfaces for food industry [11], cell proliferation in medical implants [12], friction reduction [13], enhanced antireflection [14], [15] or they act as diffraction grating exhibiting structural angle-dependent colours utilised in hologram fabrication or counterfeiting applications [16].

LIPSS appear on the material's surface as ripple-like structures after irradiation with a polarised ultrashort laser beam and their characteristic are dependent on wavelength and processing parameters. In particular, laser fluence affects ripples depth while wavelength and incidence angle has an impact on periodicity and polarisation vector influences their orientation [17]. Typically, LIPSS emerge on a surface when the fluence is much lower than the ablation threshold of a given material and a relatively small number of pulses is required. The evolution of LIPSS on processed surfaces is as follows. Firstly, random nanostructures are created with features like nano holes, nano cavities or nano protrusions. A further increase of accumulated fluence, e.g. by increasing the number of pulses and/or their fluence, leads first to High Spatial Frequency LIPSS (HSFL) that then evolve gradually from Low Spatial Frequency LIPSS (LSFL) into grooves/bumps and spikes [18]. Currently, LSFL attracts more attention as they can be easily controlled, optimised and homogenously produced on large areas and thus offer capabilities for functionalising surfaces with required repeatability for a range of applications.

So far, the LIPSS research was mostly focused on their generation and optimisation on planar surfaces because of the requirement to assess/characterise their functional response and also due to equipment related constraints. However, when the identified processing domains are applied onto non-planar surfaces, additional factors start affecting the LIPSS formation and also their functionality. These factors are disturbances that alter the processing conditions. The two most prominent ones are Beam Incident Angle (BIA) and Focal Offset Distance (FOD). Their influence on LIPSS formation was studied and it was reported that BIA mostly affects the LIPSS periodicity while FOD influences the average peak to valley amplitudes of generated ripples [19]. The presence of these disturbances can change laser processing conditions dramatically, and result in an interrupted LIPSS generation that consequently can affect the surface functional response. One way to counteract these undesirable effects when processing non-planar surfaces is to process them with a focused laser beam and always with normal incidence. However, such approach requires the use of multi-axis laser processing systems with simultaneous control of optical and mechanical axes in the beam delivery sub-system. Therefore, a more common approach is to maintain BIA and FOD within some pre-defined limits that can be determined experimentally and thus to maintain the LIPSS functional response within acceptable limits [20]. Then, such "tolerances" can be used to partition freeform surfaces, e.g. by employing so-called "freeform surface layering" [21] or by applying tessellation/triangulation

algorithms [22], [23], and thus to design and implement optimised processing techniques and strategies.

It is worth mentioning that the procedure for verifying the BIA and FOD tolerances is always material specific for a given laser processing domain and can be time-consuming. Therefore, when LIPSS surface treatments are employed in industrial applications, there are available simplified models that can be used to determine the laser processing domains for a given material and thus to produce areas covered consistently and homogenously with LIPSS [24]. However, the results are valid only for planar surfaces without taking into consideration dynamic changes in processing conditions. Therefore, there is a need for analytical methods that can determine reliably processing tolerances for producing functionalised surfaces on non-planar surfaces.

In this research, a model is proposed for assessing the accumulated fluence when processing non-planar surfaces that accounts for the disturbances affecting the processing conditions. It considers actual spatial pulse intensity distributions in the presence of varying FOD and BIA. Ultimately, by simulating the processing conditions considering the effects from these disturbances and material optical properties, the LIPSS characteristics can be predicted, i.e. their amplitudes and periodicity. Thus, it is possible to judge indirectly about LIPSS functional response on complex surfaces where otherwise their properties are difficult to measure.

2. Theory

2.1 Ultrashort laser irradiation with an astigmatic Gaussian beam

The existing models for ultrashort laser irradiation of materials usually assume an ideal Gaussian beam intensity distribution, i.e. a circular profile with symmetrical divergence above and below the focal plane, even when non-planar and inclined surfaces are processed [25]–[27]. This assumption can be acceptable in conditions where the effects of any processing disturbances can be simplified or even neglected. However, this is not the case anymore when a given laser structuring/texturing application is more sensitive to FOD and BIA variations. In addition, when laser sources are integrated into systems with relatively long beam paths incorporating several components, the beam reaching the substrate might be astigmatic. This type of Gaussian beams has two principal directions in the transversal planes. Its waists positions do not coincide and thus the beam is not always circular throughout the propagation axis and has elliptical cross-sections [28]. There are many applications where the presence of processing disturbances cannot be ignored and the actual Gaussian beam should be considered in the models. In this way, significant discrepancies in simulation results can be avoided, i.e. due to varying local fluence and pulse overlaps.

It could be assumed that the Gaussian beam is a simple astigmatic one where the ellipses of constant intensity and phase are aligned and their orientation stays constant at every point along the beam path [29]. The two-dimensional local fluence intensity distribution of such beam on a processed surface can be described using the following equation:

$$F(x,y,z) = F_0 \, exp\left(\frac{-2}{\omega_x^2(z)}x^2 + \frac{-2}{\omega_y^2(z)}y^2\right) \quad (1)$$

where F_0 is the peak fluence expressed as:

$$F_0(z) = \frac{2P}{f\pi\omega_x(z)\omega_y(z)} \tag{2}$$

where: P is average power and f - pulse repetition rate. Beam waists ω_x and ω_y of astigmatic beams depend on the position along the laser propagation axis, z, and they can be calculated as follows:

$$\omega_i(z) = \omega_{0i}\sqrt{1 + \left(\lambda\frac{z - z_{0i}}{\pi\omega_{0i}^2}M_i^2\right)^2}, i = x, y \tag{3}$$

where: ω_{0i} is the smallest waist at z_{0i}; λ – the laser wavelength, and M_i^2 – the beam quality factor for each principal direction. Astigmatism is defined as the difference between the smallest waists' position, i.e. $z_{0x} - z_{0y}$. If that distance is equal to zero, the beam is not astigmatic.

Processing of an area bigger than a beam spot size requires laser beam movements in a two-dimensional domain that is realised by employing x and y beam deflectors. The area processed with multiple pulse trains with different overlaps in x and y is depicted in Figure 1. For a given scanning speed v and f, the distance between pulses along the x equals to $\Delta x = \frac{v}{f}$ while along y is $\Delta y = h$, where h is the hatch offset between two consecutive y trains. Hence, the number of pulses along x and y when processing an area L_xx L_y can be calculated as follows:

$$N_x = \frac{L_x - 2\omega_x}{\Delta x}, N_y = \frac{L_y - 2\omega_y}{\Delta y} \tag{4}$$

It is worth stressing that these equations are valid if an assumption is made that the beam waist is constant and the laser beam is always focused on the surface. However, due to the beam astigmatism and resulting ellipticity, the smallest beam waists might not always be at the same focal position.

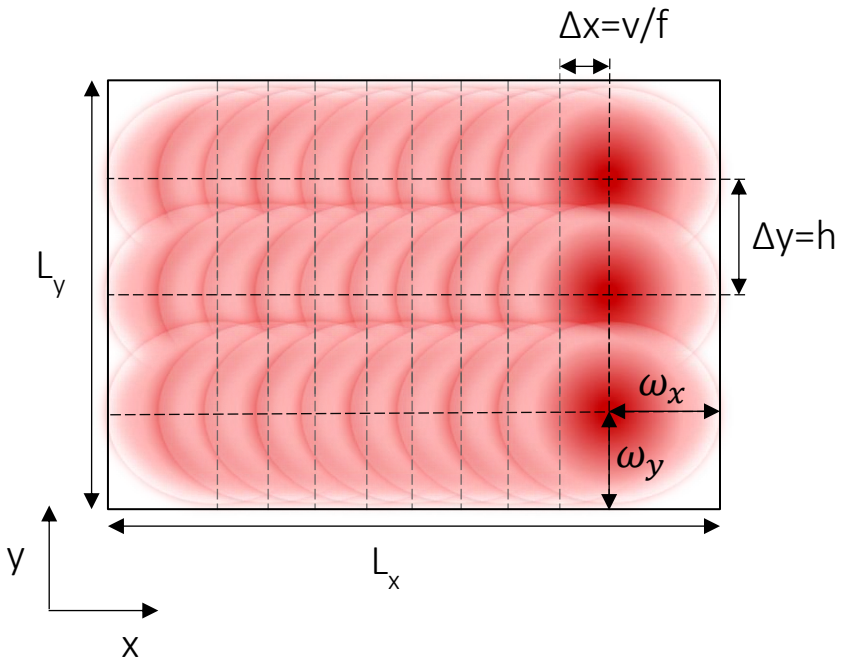

Figure 1. A schematic representation of an area L_x x L_y processed with elliptical beam spots with multiple pulse trains with pulse overlaps in x depended on the scanning speed (v) and frequency (f) while in y on hatch offset (h) between two consecutive pulse trains.

By combining Eq. 1-4, the accumulated fluence over a L_xx L_y area can be expressed by using the following equation:

$$F_{acc}(x,y,z) = N_r \frac{2P}{f\pi\omega_x(z)\omega_y(z)} \sum_i \sum_j exp\left(-2\left(\left(\frac{x-\Delta x\cdot i}{\omega_x(z)}\right)^2 + \left(\frac{y-\Delta y\cdot j}{\omega_y(z)}\right)^2\right)\right) \quad (5)$$

where: N_r is the number of passes over the area while i and j are integers in the ranges of $\left(\frac{-N_x}{2}, \frac{N_x}{2}\right)$ and $\left(\frac{-N_y}{2}, \frac{N_y}{2}\right)$, respectively, if the origin of the coordinate system is in the centre of the processed area.

2.2 The BIA effects on ultrashort laser irradiation model

As stated in Section 1, laser processing conditions vary when non-planar surfaces are processed, in particular due to BIA and FOD variations. BIA, α, is defined as the angle between the incident laser beam and the surface normal at a given point (x,y,z). For example, if an inclined planar surface is processed, BIA will be maintained the same throughout the area. In this case, to calculate the fluence intensity distribution of a single pulse, Eq. 1-3 should be revised. Figure 2 shows a schematic representation of a laser beam when processing an inclined surface. As can be seen, the beam ellipticity increases with the increase of BIA. The smaller ellipse in the figure depicts the spot size of the same beam but when it is focused on a surface normal to the beam. In this case, the BIA variations do not affect ω_x but ω_y varies and its value cannot be calculated anymore by using Eq. 3. In addition, the beam waist is now dependent on the local focal offset, Δz , and BIA, α, and this should be

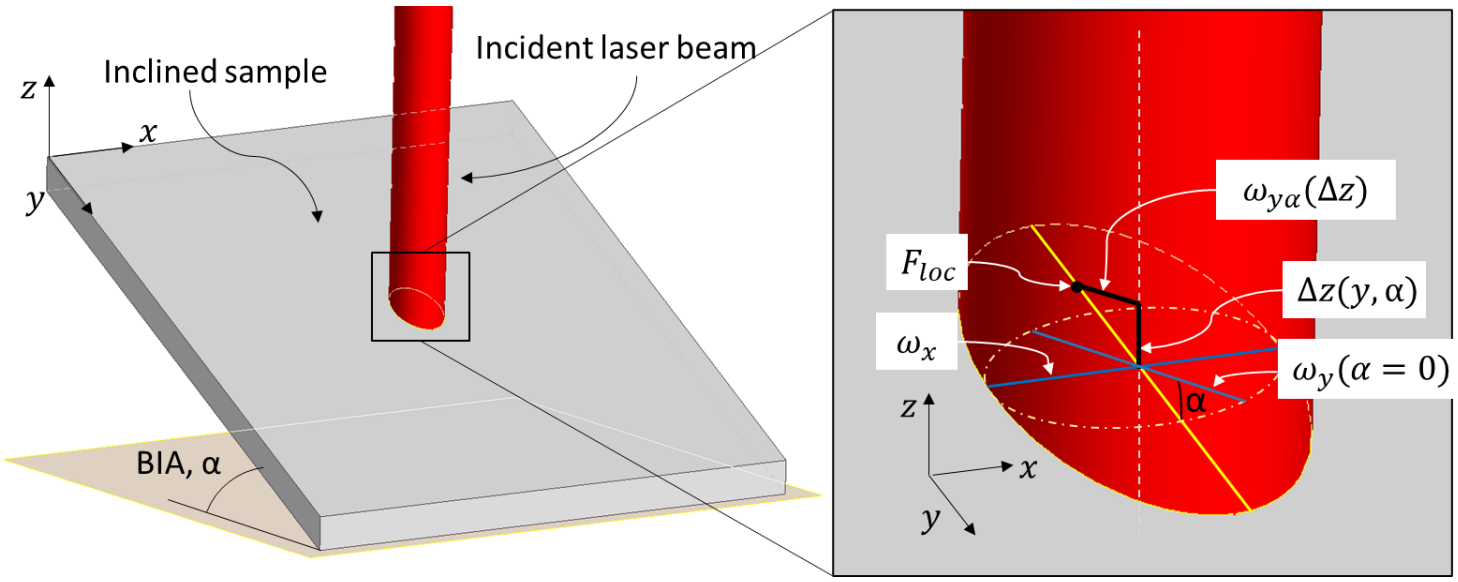

Figure 2. A schematic representation of an incident laser beam on an inclined surface. For comparison, the blue lines and smaller dash-dotted ellipse depicts the beam spot at the focal plane. The black lines represent beam waist $\omega_{y\alpha}$ and Δz necessary to calculate the local fluence F_{loc} at a given point. The bigger ellipse depicts the area where intensity is at $1/e^2$ of F_0 while the yellow line is the absolute beam diameter.

considered when calculating the local fluence (F_{loc} in Figure 2). As a result, $\omega_{y\alpha}$ increases with the distance from the pulse centre and thus Eq. 3 should be revised as follows:

$$\omega_{y\alpha}(y,z,\alpha) = \omega_{0y}\sqrt{1+\left(\lambda\frac{(z-\Delta z(y,\alpha)-z_{0y})}{\pi\omega_{0y}^2}M_y^2\right)^2} \quad (6)$$

where $\Delta z(y,\alpha) = \sin(\alpha)\cdot y$.

Considering Eq. 6, the fluence of a single pulse on an inclined surface can be calculated as follows:

$$F(x,y,z,\alpha) = \frac{2P\cos(\alpha)}{f\pi\omega_x(z)\omega_{y\alpha}(y,z,\alpha)}exp\left(-2\left(\left(\frac{x}{\omega_x(z)}\right)^2+\left(\frac{y\cos(\alpha)}{\omega_{y\alpha}(y,z,\alpha)}\right)^2\right)\right) \quad (7)$$

Examples of pulse intensity profiles are given in Figure 3a. The profiles were calculated based on Eq. 6 and 7 with $\omega_0 = 20\ \mu m$, $\lambda = 1.03\ \mu m$ and $M^2 = 1.2$ on planar and inclined surfaces, especially with

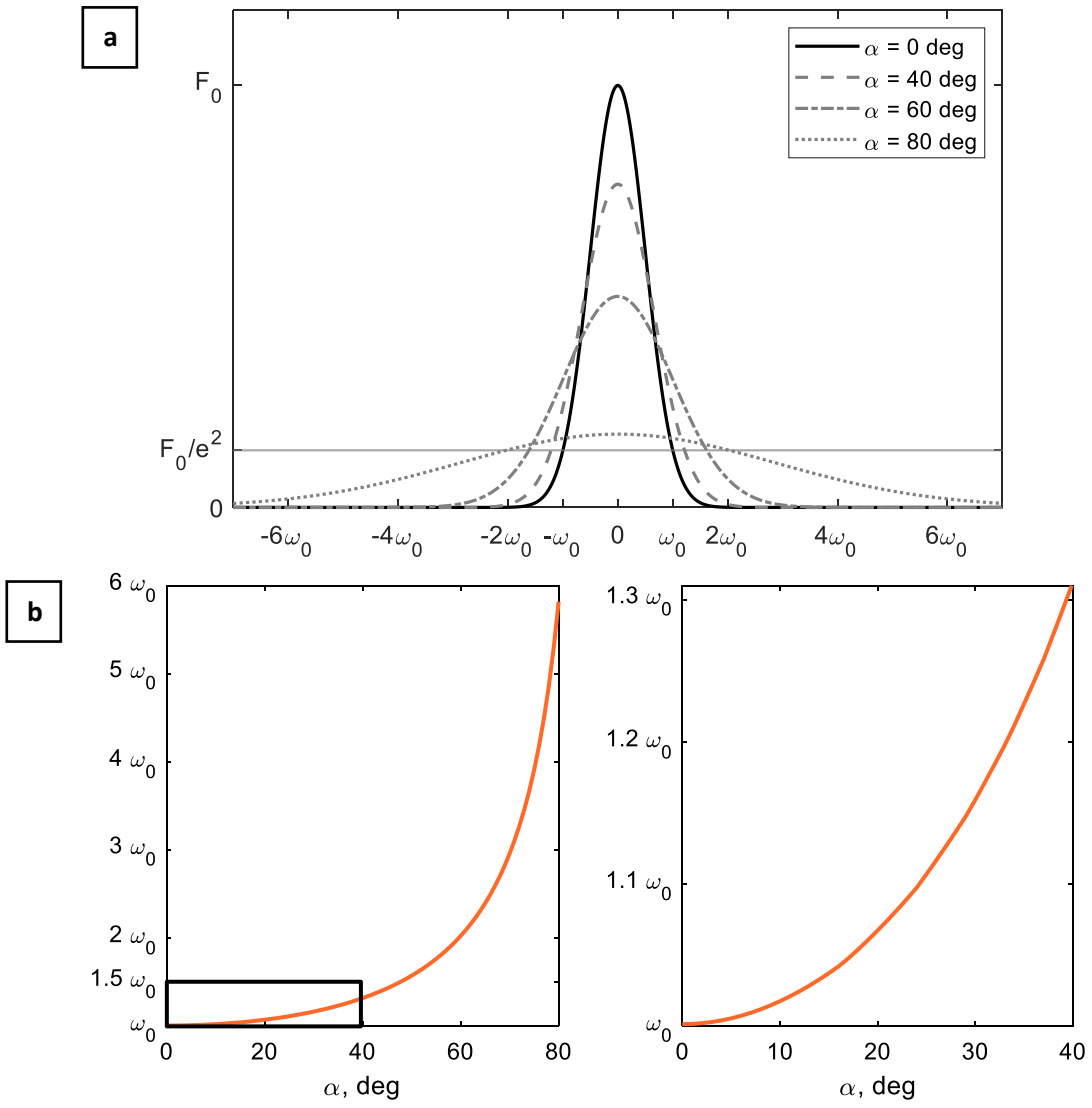

Figure 3. (a) The changes of pulse intensity profiles of a laser beam with ω_0 of 20 µm when varying BIA, **(b)** The relative changes of same beam waist when increasing BIA from 0 to 80 deg on the left; close up from 0 to 40 deg on the right.

BIA of 40, 60 and 80 degrees. The point at which the intensity drops to $1/e^2$ of also affected F_0 at given BIA determines ω_α on the processed surface. Figure 3b shows the relative changes of the same beam when varying BIA. It is apparent that the changes of the beam profile are less pronounced for BIA up to 40 deg while the difference increases up to around 30 % of ω_0. In addition, beams with different ω_0 will follow nearly the same trend for BIA changes. However, when processing a surface with a bigger BIA, ω_α increases more rapidly and for BIA = 80 deg the beam waists can be a few times bigger compared with that when it is normal to the surface. Therefore, when processing surfaces with a varying BIA, the irradiated area by each pulse increases together with the overlap between them.

Depending on the substrate, fluence values might be altered with BIA because of the absorption changes. Absorptivity, A, of metals can be estimated based on the well-known Fresnel equations with the refractive index of materials $(n + ik)$ that is wavelength dependent [30]:

$$A_p = \frac{4n\ \cos\alpha}{(n^2+k^2)\cos^2\alpha + 2n\cos\alpha + 1}$$
$$A_s = \frac{4n\ \cos\alpha}{n^2+k^2+2n\cos\alpha+\cos^2\alpha} \tag{8}$$

where: p and s denote linear p and s beam polarisations, respectively. If circular polarisation is used, absorption is an average of the two components $A_c = \frac{1}{2}(A_p + A_s)$.

Taking all these into consideration, the absorbed accumulated fluence on an inclined surface of ultrashort laser simple astigmatic Gaussian beam can be calculated as follows:

$$F_{acc}(x,y,z,\alpha) = A\ N_r \sum_i \sum_j \frac{2P\cos(\alpha)}{f\pi\omega_x(z)\omega_{y\alpha}(y,z,\alpha)} exp\left(-2\left(\left(\frac{x-\Delta x\cdot i}{\omega_x(z)}\right)^2 + \left(\frac{(y-\Delta y'\cdot j)\cos(\alpha)}{\omega_{y\alpha}(y,z,\alpha)}\right)^2\right)\right) \tag{9}$$

where: $\Delta y' = \Delta y/\cos(\alpha)$ is the distance between pulses on the surface if they are not compensated during laser scanning, in particular when the structuring strategy is based on projections [27]. Also, while calculating local distance Δz for each pulse, its displacement should be considered, thus $\Delta z(y) = \sin(\alpha)\cdot(y - \Delta y'\cdot j)$.

This model can be further generalised for processing of freeform surfaces. With the increase of surface complexity, its geometry plays a more important role in assessing the fluence distribution and accumulation. Surfaces can be clustered into developable and non-developable ones. In particular, the first are ruled surfaces, such as cylinders or cones, while the latter are compound curved surfaces, e.g. spheres, where the curvature is present in two or more directions [31]. When processing such surfaces, BIA varies in each direction and depends on the surface tangent at a given point (x, y, z) of the workpiece. Provided that the local radius of the curvature is significantly bigger than the beam waist (R>>ω), the fluence distribution of a single pulse on a freeform surface can be simplified to determine local BIA in both principal planes. Hence, BIA variations along x and y directions can be calculated as follows:

$$\alpha_k(k,z) = \frac{\pi}{2} - \tan^{-1}\left(\frac{z-z_c}{k-k_c}\right), \qquad k = x, y \tag{10}$$

where: x_c, y_c and z_c is the centre of the curvature, which radius is $R = \sqrt{(z-z_c)^2+(y-y_c)^2+(x-x_c)^2}$. Similar to Eq. 7, the fluence distribution of a single pulse on a spherical surface can be described as follows:

$$F(x,y,z,\alpha_x,\alpha_y) = F_0(x,y,z,\alpha_x,\alpha_y)\, exp\left(-2\left(\left(\frac{x\cos(\alpha_x)}{\omega_{x\alpha}(x,z,\alpha_x)}\right)^2+\left(\frac{y\cos(\alpha_y)}{\omega_{y\alpha}(y,z,\alpha_y)}\right)^2\right)\right) \quad (11)$$

Regarding the accumulated fluence, analogous to inclined surface presented before, the contributions of all pulses delivered onto the processed area need to be considered. Hence, only an iterative model can be used that is adapted to the surface complex geometry and thus assess the influence of any processing disturbances, locally.

2.3 Fluence requirements in laser structuring/texturing

Models for ultrafast laser irradiation with Gaussian beams have already been used to simulate ablation [32] and laser structuring [24], [33]. One of their main assumptions is that ablation or structuring occurs when the processing fluence is above a certain threshold, F_{th}. Furthermore, different types of morphologies, i.e. laser induced structures, appear if processing is carried out within a predefined fluence range. Previous studies shows that, for multi-pulse structuring, with the increase of the pulse number, N_p, impinging a given spot the fluence thresholds can be reduced [34]. This is attributed to a material dependent incubation phenomenon and can be expressed in the power-law form:

$$F_{th}(N_p) = F_{th}(1)N_p^{S-1} \quad (12)$$

where: $S \in [0,1]$ is an incubation factor and $F_{th}(1)$ is the fluence threshold for a single pulse. The incubation model can also describe the relationship between the accumulated fluence threshold, $F_{acc\,th}$, and N_p as a requirement to achieve a certain morphology on the surface [24]:

$$F_{acc\,th}(N_p) = F_{th}(N_p)N_p = F_{th}(1)N_p^S \quad (13)$$

However, when beams are being scanned across a given surface area and pulses' overlap, assessing the number of pulses per spot have to be estimated and then used for threshold calculations. Thus, the effective number of pulses can be calculated as follows [33]:

$$N_{p\,eff} = \frac{\pi}{2}\frac{\omega_x\omega_y}{\Delta x\Delta y} \quad (14)$$

Please note that depending on the chosen scanning strategy and the complexity of workpiece geometry, the beam spot size is not constant anymore throughout the processed field, as has been shown in Section 2.2. This leads to increased impact of processing disturbances, i.e. BIA and FOD variations, and as a result, it will also influence the local fluence threshold variations that have to be accounted for when calculating F_{acc}.

3. Methodology

3.1 Experimental setup and materials

Experimental validation was performed using ultrafast Ytterbium-doped laser source with a pulse duration of 310 fs, maximum pulse energy of 10 µJ, a near-infrared wavelength (λ) of 1032 nm, and maximum average power of 5W. A linearly polarised laser beam was focused with a 100 mm

telecentric lens which allows always normal incidence within the field of view. The laser processing of surfaces was realized by employing a 3D scan head. Additionally, a motorized rotational axis was employed to control BIA. The test workpiece on which LIPSS were created was 1.5 mm thick, mirror polished, 304 stainless steel plate. It was cleaned with acetone before the laser processing. The complex refractive index of this material for the employed laser source was (2.943 + 3.915*i*) [35] and this value was used in the calculations.

3.2 Beam characterisation

Beam waist measurements along the beam propagation axis were conducted using a scanning slit beam profiler. Each measurement was repeated three times with an increment of 100 µm along z. Results from beam waist measurements are provided in Figure 4. The values were fitted to Eq. 3 using least squares method assuming that z_{0i}, ω_{0i} and M_i^2 were variables and λ was constant. The peak fluence is the highest at the focal plane where the area the beam spot size is the smallest. The astigmatism of the used laser beam was 0.52 mm and the focal plane did not coincide with z_0 along x and y axis and were equal to -0.41 mm and 0.11 mm, respectively. The smallest waists, i.e. ω_{0x} and ω_{0y}, at these positions were 20.52 and 16.52 µm, respectively, while in the focal plane, ω_x and ω_y were equal to 22.33 µm and 16.82 µm, correspondingly. Beam propagation factor, M^2, that also characterizes the deviation of the ideal Gaussian beam in the fundamental mode was calculated to be 1.35 and 1.45 in x and y, respectively. That means that the beam's divergence half-angle differs in both directions and was 21.6 mrad and 28.8 mrad. It is worth mentioning that the beam spot size area, and thus peak fluence, along the propagation axis was not symmetrical and therefore this could lead to different processing conditions below and above the focal plane. Such initial characterization of the laser beam can be used in the model that also accounts for disturbances that occur during processing of free form surfaces, such as BIA and FOD variations.

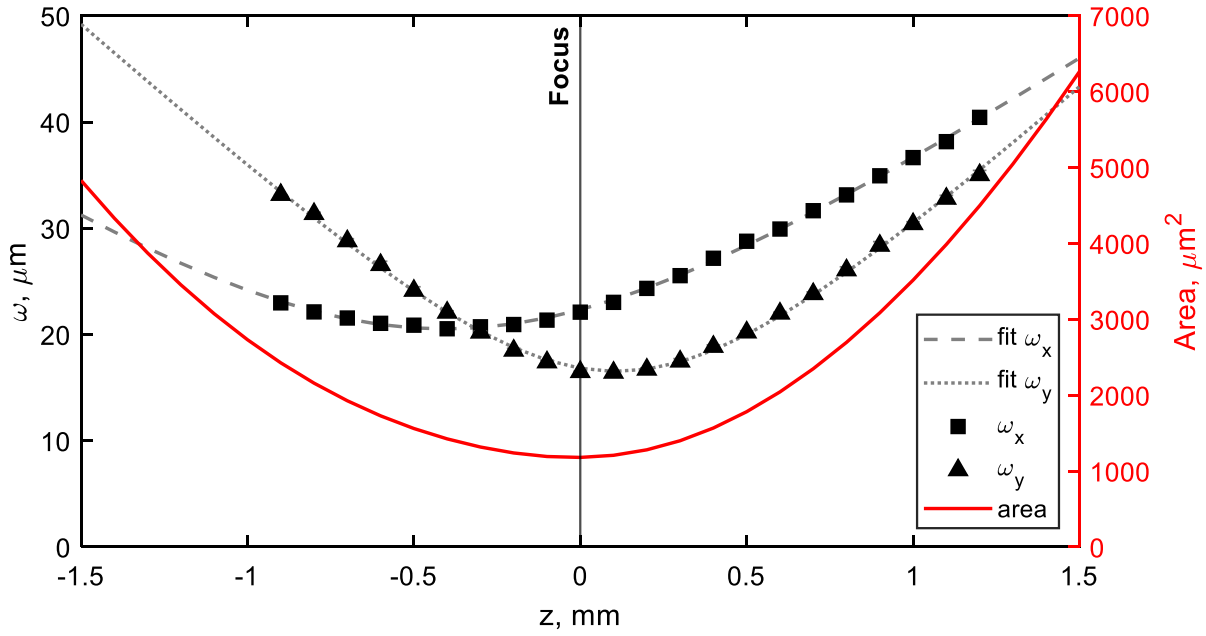

Figure 4. Beam waist measurements along the propagation axis, z, in two principal directions, i.e. x and y, and their fitted curves to Eq. 3. The red line represents the changes of beam spot area along z.

3.3 Experimental validation

A field of 4x4 mm was scanned with a linearly p-polarised laser beam in a way that both disturbances, i.e. BIA and FOD variations, were present and controlled as depicted in Figure 5. The laser beam was focused at one end of the square on the inclined sample and as the laser scanning progressed in y, FOD was increasing with each $\Delta y = 6\ \mu m$ displacement. As a result, actual $\Delta y'$ on the sample was not compensated and differed for each BIA used in this experimental study, i.e. 10, 20, 30 and 40 deg. The repetition rate used was 500 kHz while the scanning speed was adjusted to 2000 mm/s and thus to maintain a pulse distance of $\Delta x = 4\ \mu m$. Initially, the LIPSS fluence threshold and the relation between fluence and LIPSS depth was determined when disturbances were not present, and this yielded constant $N_{p\ eff}$ of 24.6.

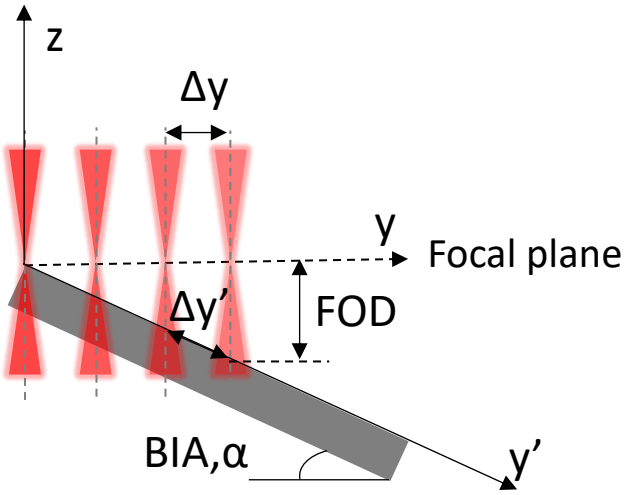

Figure 5. A schematic representation of the employed scanning strategy on test samples where both disturbances, i.e. BIA and FOD are present and controlled.

LIPSS were characterised with an Atomic Force Microscope (AFM). The samples produced without disturbances were measured three times in different locations while the validation samples were scanned along a straight line in y' every 250 µm, until LIPSS were still present. Ripples' geometric characteristics were obtained by using the open source software Gwyddion. From each 20 x 20 um (256 x 256 px) AFM scan, five lines, 2.3 µm (30 px) wide, were drawn perpendicular to LIPSS profiles. LIPSS amplitudes were expressed as standardised roughness parameter Rtm, that describes an average distance between the highest peak and lowest valley in every sampling length. Additionally, for each scan 2D Power Spectral Density Function (2D PSDF) was performed based on 2D Fast Fourier Transformation (2D FFT) in order to evaluate characteristic spatial frequencies, occurring in LIPSS covered surface, from which periodicity was obtained.

LIPSS periodicities were calculated based on the theory of ripples generation with excitation of surface electromagnetic waves. In particular, it incorporates laser incidence on the surface, laser source wavelength (λ) as well as the polarisation type and complex dielectric constants of medium, ε_1, and the processed material, ε_2 [36]. Throughout the experiments the p-type polarisation was utilised, hence the theoretical LIPSS periodicity was determined as follows:

$$\Lambda_{p\pm} = \frac{\lambda}{Re\sqrt{\frac{\varepsilon_1\varepsilon_2}{\varepsilon_1+\varepsilon_2}} \pm \sin\alpha} \quad (15)$$

As the equation indicates, LIPSS produced with p-polarisation and with not normal incidence have two superimposed periodicities and are referred to + or – as for the sign used in the calculations. Dielectric constants employed in the calculations were ε_1= (1+0i) and ε_2 = (-7.636 + 27.175*i*) for air and steel, respectively [37].

4. Results and discussion

4.1 LIPSS characteristics vs. accumulated fluence

Initial experiments were conducted without the presence of any disturbances on the planar surface to study relations between LIPSS geometrical characteristics and the accumulated fluence. Only pulse energy was varied and thus, the accumulated fluence was affected by the changes in the peak fluence. As can be seen in Figure 6a, LIPSS amplitudes rapidly increase to 150 nm after the fluence threshold of approximately 0.11 J/cm^2, and then slowly continue to rise with the increase of the peak fluence. Above F_0 = 0.5 J/cm^2, LIPSS became noticeably irregular and were not considered homogenous anymore. In regard to the LIPSS periodicity, Λ, in Figure 6b, it was between 900 and 930 nm on average and it can be considered unaffected within the range of peak fluence studied in this research.

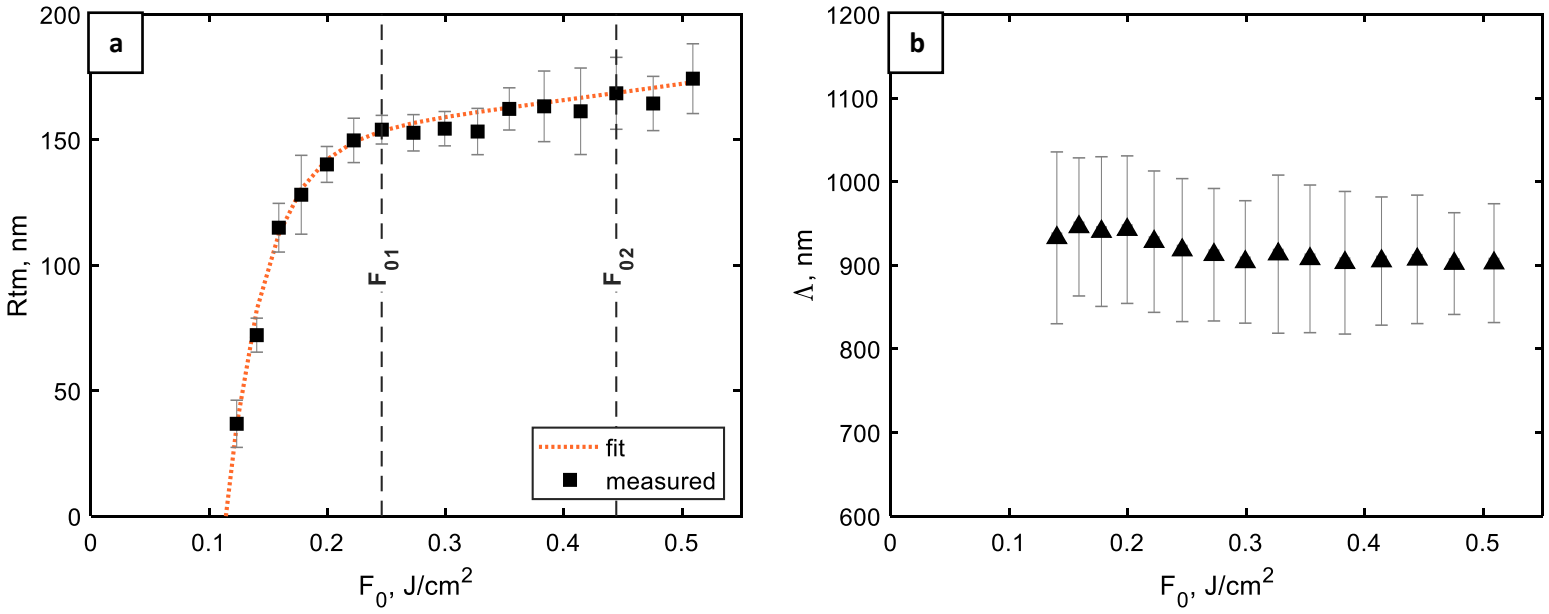

Figure 6. Dependence of LIPSS amplitudes **(a)** and periodicity **(b)** with F_0 increase. Two vertical lines in **(a)** indicate peak fluences used in validation samples fabrication.

For the sake of simplicity, an empirical equation was fitted to the measured data in Figure 6a, that described the changes of LIPSS amplitudes with the increase of the peak fluence. Based on the same input data, the processing conditions were simulated and previously identified F_{th} was then used to assess F_{acc}. In the context of the freeform surface processing, this interdependence can be used to predict the processing settings that would lead to a significant decrease of F_{acc} and thus to the loss

of LIPSS surface characteristics, i.e. a significant drop in the peak-to-valley distance. In particular, it is critical to identify the gradient between F_{th} and the fluence at which the surface structures can reach their optimum characteristics and ultimately functional response. By applying this approach, processing tolerances in regard to processing disturbances can be estimated and consequently the sizes of processed fields in freeform laser structuring/texturing can be optimized. To validate the model, two F_0 were used and they are highlighted in Figure 6a. In particular, F_{01} = 0.25 J/cm^2 was used for the optimised laser setting for producing LIPSS and F_{02} = 0.44 J/cm^2 where ripples are still homogenous and with a higher reserve of fluence in regards to F_{th}.

4.2 Model validation

As discussed in Section 2.3, the presence of disturbances leads to variations of the local beam waist and thus the local fluence threshold varies, too. Therefore, to assess F_{acc} only the local fluence from each pulse above the threshold was taken into account when simulating the process. Another reason for this was to avoid very small fluence values to affect final F_{acc} that do not have any physical effect on the laser structuring process. The incubation factor utilized in the process simulation was S = 0.86, with $F_{th}(1)$ = 0.179 J/cm^2, which is the typical value for 304 stainless steel if $N_{p\,eff}$ < 1000 is used [38].

Figure 7 shows the experimental results in regard to the resulting LIPSS amplitudes and their predicted values based on F_{acc} along y'. It can be stated that the ripples, especially at the upper end of the

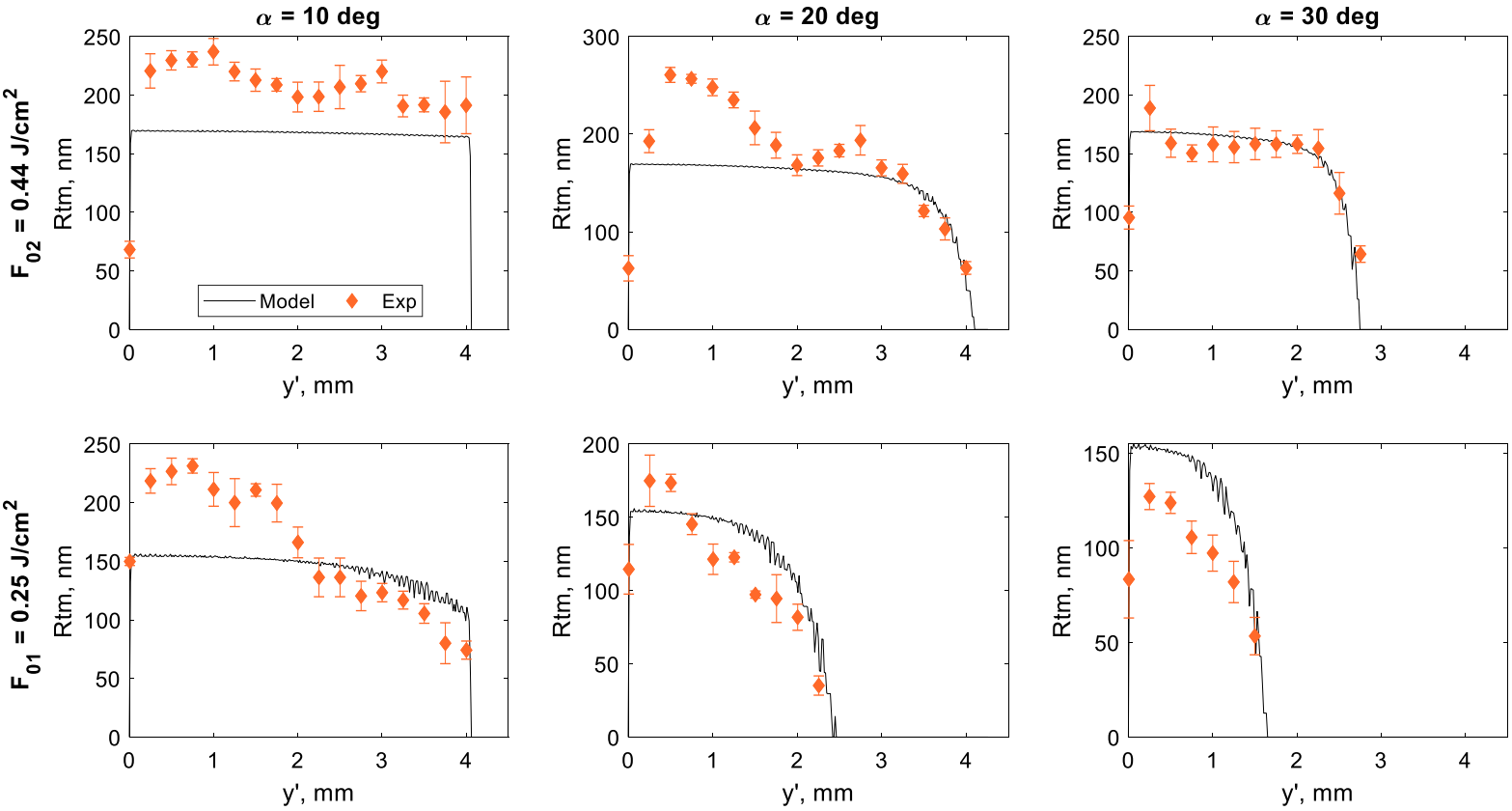

Figure 7. Experimental measurements of LIPSS amplitudes vs. their predicted values based on calculations of F_{acc} along y' for BIA of 10, 20 and 30 deg, and also for initial F_{01} of 0.25 J/cm^2 (bottom row) and F_{02} of 0.44 J/cm^2 (top row).

processed square field, where they were mostly influenced by the BIA deviation from normal and not as much by FOD, were typically deeper when compared to LIPSS produced with a beam normal to the surface. It should be noted that the LIPSS formation mechanism is more complex [39] and therefore some aspects were not taken into account in the relatively simple model presented in Section 2. However, in spite of this, it was possible to predict the location where the ripples are not anymore generated on the surface in all six cases depicted in Figure 7. In particular, this was done by calculating the LIPSS amplitudes that decreased with the drop of F_{acc} caused by processing disturbances. The area with LIPSS present on the processed fields decreased with the increase of the BIA while the FOD influence was more pronounced. The impact of the initial pulse energy was also visible. LIPSS of similar depth could be maintained onto a bigger area for F_{02} than F_{01}.

Regarding the LIPSS periodicity, Figure 8 shows that mostly both Λ_{p-} and Λ_{p+} were present, as explained in Section 2.3. Despite the changes in processing conditions caused by the disturbances, i.e. increase of beam spot size and consequently the decrease of the peak fluence on the processed surface, no major Λ variations were observed. This could be attributed to the fact that the pulse energy was maintained constant. Moreover, the increase of BIA led to Λ_{p-} with lower values than the theoretical ones. This phenomena was already studied by researchers and it was explained with the increased influence of the surface roughness induced by the laser pulses that impacted the ripples periodicity [40]. In addition, Λ_{p+} was not always present on the processed fields, e.g. for F_{02} and BIA of 10 deg, smaller ripples emerged on the surface at y' = 2.5 mm, while at 20 deg, it was only at y' of 1.5 mm. Besides, at the upper end of the processed field where F_{acc} was higher, Λ_{p-} was always the more dominant periodicity than Λ_{p+} and with the decrease of F_{acc} along y' this tendency began to shift. The evolution of LIPSS Λ is depicted in Figure 9 that shows three AFM scans from the same field processed with F_{02} and at BIA of 20 deg. At y' of 0.75 mm, only a higher Λ_{p-} could be seen while at 1.5 mm a mix of both periodicities is detectable. The last image taken at y' = 3.5 mm shows only the presence of Λ_{p+}. This suggests that these periodicities are also sensitive to changes of F_{acc}. The 2D PSDF analysis of each AFM scans for this particular sample is presented in Figure 10 and now Λ

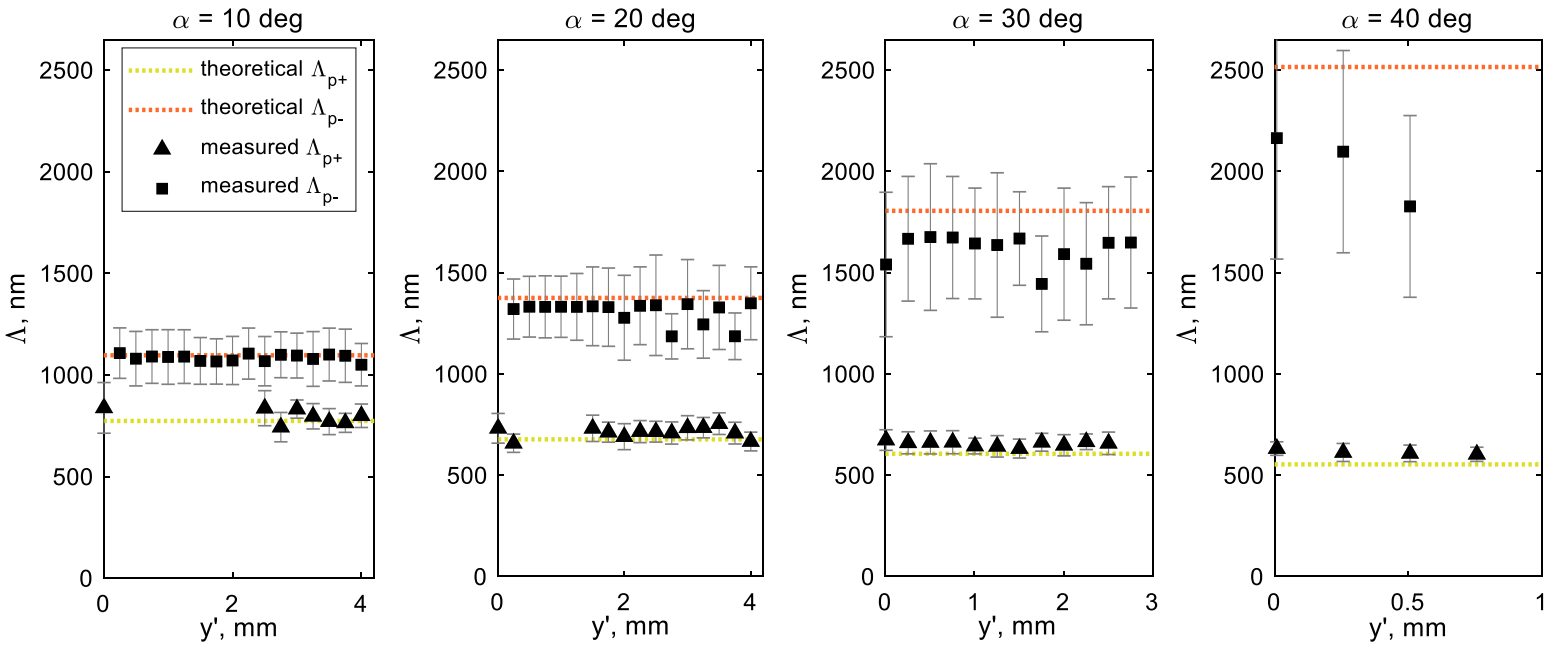

Figure 8. Measured LIPSS periodicities Λ_{p-} and Λ_{p+} and their theoretical values (from Eq. 15) for samples produced with F_{02} = 0.44 J/cm^2 and BIA of 10, 20, 30 and 40 deg.

magnitude in regard to F_{acc} can be analysed. Especially, there is a clear trend that with the increase of the distance from the top of the processed field, the significance of Λ_{p-} decreases. Furthermore, the processing conditions when Λ_{p-} becomes inferior to Λ_{p+} are reached when F_{acc} is approximately 6 J/cm^2 and below and they are the same for the rest of the tested samples produced with F_{02} while for F_{01} this value was above 2 J/cm^2. It can imply that different fluence thresholds need to be recognized for these LIPSS characteristics and further research should be conducted to confirm this.

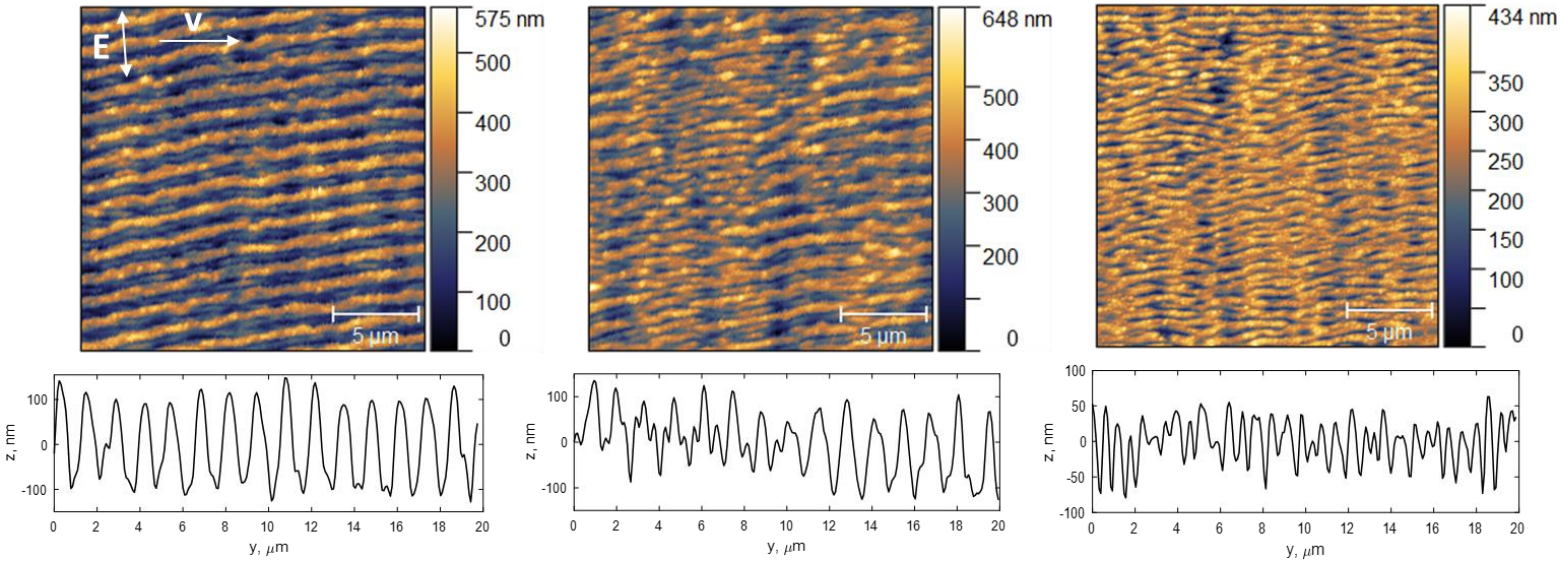

Figure 9. AFM scans of a sample produced with F_{02} = 0.44 J/cm^2 and BIA 20 deg along y' at 0.75 mm (left), 1.5 mm (middle) and 3.5 mm (right) with their respective profiles. White arrows indicate direction of polarisation vector (E) and scanning direction (v).

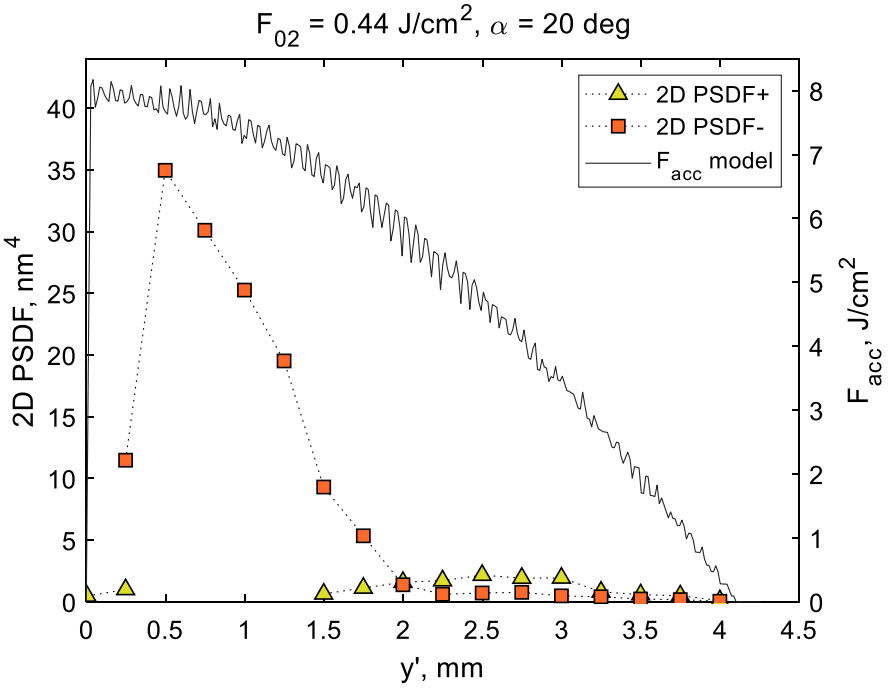

Figure 10. Measured PSDF values for sample produced with F_{02} = 0.44 J/cm^2 and BIA 20 deg along y' and calculated F_{acc} profile for this processing settings.

5. Conclusions

In this research, an ultrafast laser irradiation model for structuring free form surfaces was proposed. A simple astigmatic Gaussian beam was considered in assessing the accumulated fluence during structuring surfaces with varying BIA, i.e. inclined and curved ones. It was demonstrated that surfaces structured with processing disturbances, such as BIA and FOD, the pulse fluence distribution changes and results in modifications of laser processing conditions, in particular beam size variations that affect local fluence thresholds.

Validation samples were produced with varying BIA, i.e. on an inclined surface, where both disturbances were present and controlled. It was shown that the LIPSS characteristics, i.e. amplitudes and periodicity, can be predicted by modelling the accumulated fluence on a field processed with a characterised laser beam. Namely, the LIPSS disappearance or transformations due to the presence of BIA and FOD variations can be predicted. Furthermore, changes in LIPSS behaviour can be predicted, too, and thus to determine the processing constraints for a given laser parameters' domain without conducting the necessary empirical studies. Such information then can be used to drive the partitioning of freeform surfaces into laser processing fields and thus to achieve the required LIPSS homogeneity and consistency in their functional response.

Acknowledgement

The work was carried out within the H2020 FoF programme "High-Impact Injection Moulding Platform for mass-production of 3D and/or large micro-structured surfaces with Antimicrobial, Self-cleaning, Anti-scratch, Anti-squeak and Aesthetic functionalities" (HIMALAIA), the ITN programme "European ESRs Network on Short Pulsed Laser Micro/Nanostructuring of Surfaces for Improved Functional Applications" (Laser4Fun) and the UKIERI DST programme "Surface functionalisation for food, packaging, and healthcare applications". Also, the authors would like to thank the Manufacturing Technology Centre (MTC) for the financial support of Aleksandra Michalek's PhD research.

References

[1] M. Birnbaum, "Semiconductor surface damage produced by Ruby lasers," *J. Appl. Phys.*, vol. 36, no. 11, pp. 3688–3689, 1965, doi: 10.1063/1.1703071.

[2] S. Höhm, A. Rosenfeld, J. Krüger, and J. Bonse, "Laser-induced periodic surface structures on titanium upon single- and two-color femtosecond double-pulse irradiation," *Opt. Express*, vol. 23, no. 20, p. 25959, 2015, doi: 10.1364/oe.23.025959.

[3] K. Okamuro, M. Hashida, Y. Miyasaka, Y. Ikuta, S. Tokita, and S. Sakabe, "Laser fluence dependence of periodic grating structures formed on metal surfaces under femtosecond laser pulse irradiation," *Phys. Rev. B - Condens. Matter Mater. Phys.*, vol. 82, no. 16, pp. 1–5, 2010, doi: 10.1103/PhysRevB.82.165417.

[4] G. Li *et al.*, "Evolution of aluminum surface irradiated by femtosecond laser pulses with different pulse overlaps," *Appl. Surf. Sci.*, vol. 276, pp. 203–209, 2013, doi: 10.1016/j.apsusc.2013.03.067.

[5] H. Hiraoka, "Pulsed laser processings of polymer and ceramic surfaces," *J. Photopolym. Sci. Technol.*, vol. 10, no. 2, pp. 205–210, 1997, doi: 10.2494/photopolymer.10.205.

[6] W. Zhang, G. Cheng, X. D. Hui, and Q. Feng, "Abnormal ripple patterns with enhanced regularity and continuity in a bulk metallic glass induced by femtosecond laser irradiation," *Appl. Phys. A Mater. Sci. Process.*, vol. 115, no. 4, pp. 1451–1455, 2014, doi: 10.1007/s00339-013-8062-z.

[7] S. Gräf, C. Kunz, and F. A. Müller, "Formation and properties of laser-induced periodic surface structures on different glasses," *Materials (Basel).*, vol. 10, no. 8, 2017, doi: 10.3390/ma10080933.

[8] M. Csete, S. Hild, A. Plettl, P. Ziemann, Z. Bor, and O. Marti, "The role of original surface roughness in laser-induced periodic surface structure formation process on poly-carbonate films," *Thin Solid Films*, vol. 453–454, pp. 114–120, 2004, doi: 10.1016/j.tsf.2003.11.086.

[9] A. Y. Vorobyev and C. Guo, "Multifunctional surfaces produced by femtosecond laser pulses," *J. Appl. Phys.*, vol. 117, no. 3, 2015, doi: 10.1063/1.4905616.

[10] G. W. Römer, D. A. Del Cerro, R. C. J. Sipkema, M. N. W. Groenendijk, and A. J. Huis In 't Veld, "Ultra short pulse laser generated surface textures for anti-ice applications in aviation," *ICALEO 2009 - 28th Int. Congr. Appl. Lasers Electro-Optics, Congr. Proc.*, vol. 102, no. 2009, pp. 30–37, 2009, doi: 10.2351/1.5061570.

[11] A. H. A. Lutey *et al.*, "Towards laser-textured antibacterial surfaces," *Sci. Rep.*, vol. 8, no. 1, pp. 1–10, 2018, doi: 10.1038/s41598-018-28454-2.

[12] L. Orazi *et al.*, "Osteoblast cell response to LIPSS-modified Ti-implants," *Key Eng. Mater.*, vol. 813 KEM, pp. 322–327, 2019, doi: 10.4028/www.scientific.net/KEM.813.322.

[13] Z. Wang, Q. Zhao, and C. Wang, "Reduction of friction of metals using laser-induced periodic surface nanostructures," *Micromachines*, vol. 6, no. 11, pp. 1606–1616, 2015, doi: 10.3390/mi6111444.

[14] P. Gecys, A. Vinciunas, M. Gedvilas, A. Kasparaitis, R. Lazdinas, and G. Raciukaitis, "Ripple Formation by Femtosecond Laser Pulses for Enhanced Absorptance of Stainless Steel," *JLMN-Journal of Laser Micro/Nanoengineering*, vol. 10, no. 2, pp. 124–128, 2015, doi: 10.2961/jlmn.2015.0.

[15] Z. Ou, M. Huang, and F. Zhao, "The fluence threshold of femtosecond laser blackening of

metals: The effect of laser-induced ripples," *Opt. Laser Technol.*, vol. 79, pp. 79–87, 2016, doi: 10.1016/j.optlastec.2015.11.018.

[16] T. Jwad, P. Penchev, V. Nasrollahi, and S. Dimov, "Laser induced ripples' gratings with angular periodicity for fabrication of diffraction holograms," *Appl. Surf. Sci.*, vol. 453, no. 1, pp. 449–456, 2018, doi: 10.1016/j.apsusc.2018.04.277.

[17] C. Yao *et al.*, "Polarization and fluence effects in femtosecond laser induced micro/nano structures on stainless steel with antireflection property," *Appl. Surf. Sci.*, vol. 425, pp. 1118–1124, 2017, doi: 10.1016/j.apsusc.2017.07.157.

[18] S. V. Kirner *et al.*, "Mimicking bug-like surface structures and their fluid transport produced by ultrashort laser pulse irradiation of steel," *Appl. Phys. A Mater. Sci. Process.*, vol. 123, no. 12, pp. 1–13, 2017, doi: 10.1007/s00339-017-1317-3.

[19] A. Michalek, T. Jwad, P. Penchev, T. L. See, and S. Dimov, "Inline LIPSS Monitoring Method Employing Light Diffraction," *J. Micro Nano-Manufacturing*, vol. 8, no. 1, Mar. 2020, doi: 10.1115/1.4045681.

[20] A. Batal *et al.*, "Effects of laser processing conditions on wettability and proliferation of Saos-2 cells on CoCrMo alloy surfaces," *Adv. Opt. Technol.*, vol. 9, no. 1–2, pp. 67–78, 2020, doi: 10.1515/aot-2019-0051.

[21] M. Jiang, X. Wang, S. Ke, F. Zhang, and X. Zeng, "Large scale layering laser surface texturing system based on high speed optical scanners and gantry machine tool," *Robot. Comput. Integr. Manuf.*, vol. 48, no. 1037, pp. 113–120, 2017, doi: 10.1016/j.rcim.2017.03.005.

[22] G. Cuccolini, L. Orazi, and A. Fortunato, "5 Axes computer aided laser milling," *Opt. Lasers Eng.*, vol. 51, no. 6, pp. 749–760, 2013, doi: 10.1016/j.optlaseng.2013.01.015.

[23] A. Batal, A. Michalek, P. Penchev, A. Kupisiewicz, and S. Dimov, "Laser processing of freeform surfaces: A new approach based on an efficient workpiece partitioning strategy," *Int. J. Mach. Tools Manuf.*, p. 103593, 2020, doi: 10.1016/j.ijmachtools.2020.103593.

[24] J. Eichstädt, G. R. B. E. Römer, and A. J. Huis In 'T Veld, "Determination of irradiation parameters for laser-induced periodic surface structures," *Appl. Surf. Sci.*, vol. 264, pp. 79–87, 2013, doi: 10.1016/j.apsusc.2012.09.120.

[25] B. Bachy, R. Süß-Wolf, T. Kordass, and J. Franke, "Simulation and experimental investigation for the 2D and 3D laser direct structuring process," *Int. J. Adv. Manuf. Technol.*, vol. 89, no. 5–8, pp. 1591–1602, 2017, doi: 10.1007/s00170-016-9173-4.

[26] L. Overmeyer, J. F. Duesing, O. Suttmann, and U. Stute, "Laser patterning of thin film sensors on 3-D surfaces," *CIRP Ann. - Manuf. Technol.*, vol. 61, no. 1, pp. 215–218, 2012, doi: 10.1016/j.cirp.2012.03.087.

[27] X. Wang, J. Duan, M. Jiang, S. Ke, B. Wu, and X. Zeng, "Study of laser precision ablating texture patterns on large-scale freeform surface," *Int. J. Adv. Manuf. Technol.*, vol. 92, no. 9–12, pp. 4571–4581, 2017, doi: 10.1007/s00170-017-0413-z.

[28] T. Tari and P. Richter, "Correction of astigmatism and ellipticity of an astigmatic Gaussian laser beam by symmetrical lenses," *Opt. Quantum Electron.*, vol. 24, no. 9, pp. 865–872, 1992, doi: 10.1007/BF01588591.

[29] E. Kochkina, G. Wanner, D. Schmelzer, M. Tröbs, and G. Heinzel, "Modeling of the general astigmatic Gaussian beam and its propagation through 3D optical systems," *Appl. Opt.*, vol. 52, no. 24, pp. 6030–6040, 2013, doi: 10.1364/AO.52.006030.

[30] D. Bergström, “The absorption of laser light by rough metal surfaces,” Luleå University of Technology, 2008.

[31] G. Farin, “A - Quick Reference of Curve and Surface Terms,” in *Curves and Surfaces for CAGD*, 5th ed., San Francisco: Morgan Kaufmann, 2002, pp. 437–444.

[32] A. Žemaitis, M. Gaidys, M. Brikas, P. Gečys, G. Račiukaitis, and M. Gedvilas, “Advanced laser scanning for highly-efficient ablation and ultrafast surface structuring: experiment and model,” *Sci. Rep.*, vol. 8, no. 1, Dec. 2018, doi: 10.1038/s41598-018-35604-z.

[33] M. Mezera and G. R. B. E. Römer, “Model based optimization of process parameters to produce large homogeneous areas of laser-induced periodic surface structures,” *Opt. Express*, vol. 27, no. 5, p. 6012, 2019, doi: 10.1364/oe.27.006012.

[34] Y. Jee, M. F. Becker, and R. M. Walser, “Laser-induced damage on single-crystal metal surfaces,” *J. Opt. Soc. Am. B*, vol. 5, no. 3, p. 648, 1988, doi: 10.1364/josab.5.000648.

[35] P. B. Johnson and R. W. Christy, “Optical constants of transition metals: Ti, V, Cr, Mn, Fe, Co, Ni, and Pd,” *Phys. Rev. B*, vol. 9, no. 12, pp. 5056–5070, 1974, doi: 10.1103/PhysRevB.9.5056.

[36] A. M. Prokhorov, A. S. Svakhin, V. A. Sychugov, A. V Tischenko, and A. A. Khakimov, “Excitation and resonant transformation of a surface electromagnetic wave during irradiation of a solid by high-power laser radiation,” *Sov. J. Quantum Electron.*, vol. 13, no. 568, 1983.

[37] M. A. Ordal, R. J. Bell, R. W. Alexander, L. A. Newquist, and M. R. Querry, “Optical properties of Al, Fe, Ti, Ta, W, and Mo at submillimeter wavelengths,” *Appl. Opt.*, vol. 27, no. 6, p. 1203, 1988, doi: 10.1364/ao.27.001203.

[38] F. Di Niso, C. Gaudiuso, T. Sibillano, F. P. Mezzapesa, A. Ancona, and P. M. Lugarà, “Role of heat accumulation on the incubation effect in multi-shot laser ablation of stainless steel at high repetition rates,” *Opt. Express*, vol. 22, no. 10, p. 12200, 2014, doi: 10.1364/oe.22.012200.

[39] F. Fraggelakis, G. Mincuzzi, J. Lopez, I. Manek-Hönninger, and R. Kling, “Controlling 2D laser nano structuring over large area with double femtosecond pulses,” *Appl. Surf. Sci.*, vol. 470, no. November 2018, pp. 677–686, 2019, doi: 10.1016/j.apsusc.2018.11.106.

[40] Y. Fuentes-Edfuf *et al.*, “Tuning the period of femtosecond laser induced surface structures in steel: From angled incidence to quill writing,” *Appl. Surf. Sci.*, vol. 493, pp. 948–955, Nov. 2019, doi: 10.1016/j.apsusc.2019.07.106.